JOURNAL OF MATERIALS SCIENCE 27 (1992) 1537–1545

Time-dependent elastic modulus recovery measurement on thermally shocked SiC fibre–aluminosilicate composites, machinable glass ceramics and polycrystalline alumina

Y. KIM, E. D. CASE
Department of Metallurgy, Mechanics and Materials Science, Michigan State University, East Lansing, MI 48824, USA

Time-dependent partial recoveries in Young's modulus were observed for thermally shocked specimens of three ceramic materials: an SiC fibre–aluminosilicate composite, a machinable glass–ceramic, and a polycrystalline alumina. The observed Young's modulus recovery is likely to be due to room-temperature microcrack healing. The room-temperature modulus recovery rates measured in this study are compared to the physical property recovery rates obtained from an analysis of data in the literature for other cracked ceramics.

1. Introduction

Microcracks in monolithic ceramics and ceramic composites may be generated by many mechanisms including thermal expansion mismatch [1, 2], thermal shock [3], phase changes [4, 5], grinding and mechanical impact [6–8]. Experimental studies have documented microcrack-induced changes in a diverse range of properties such as strength [9, 10], elastic modulus [11–16], internal friction [11–16] and optical transparency [12].

In addition to microcrack-generation studies, numerous studies show that microcracks also can be healed [17–40]. However, microcrack healing is typically observed in terms of high-temperature diffusive healing, that is, for temperatures above a homologous temperature of about 0.6 [18–30]. Microcrack and macrocrack healing in ceramics have been observed at or near room temperature, mainly in glass [33–35, 37–39] and mica [31, 32, 37], and only recently for a polycrystalline ceramic [40]. This study considers partial room-temperature microcrack healing in three different thermally shocked ceramic materials.

2. Experimental procedure

2.1. Materials tested

The three materials employed in this study included an SiC fibre-reinforced aluminosilicate, a commercial glass–ceramic, and a polycrystalline alumina. The SiC fibre-reinforced aluminosilicate (AS) glass–ceramic composites were fabricated by Corning Glass Works using a 35 vol % loading of Nicalon fibres (Nippon Carbon Co.). The glass–ceramic specimens were prepared from commercial Macor machinable glass–ceramic (Corning code 9658) with the microstructure of randomly dispersed fluoromica platelets (approximately 10 μm across and 1 μm thick) in a glass–ceramic matrix. The polycrystalline alumina (AD-96, Coors Ceramics) specimens had an average grain size of approximately 6 to 7 μm and a density of 86.7 to 93.5% of the theoretical density.

Specimens of each of the three materials were cut into prismatic bars using a low-speed diamond saw (Table I). Prior to testing, the as-cut specimens of SiC fibre-reinforced aluminosilicate and the commercial Macor glass–ceramic specimens were thermally annealed in air at 500 °C for approximately 12 h. The polycrystalline alumina specimens were annealed in air at 850 °C for approximately 12 h. The thermal anneals helped to reduce residual stresses that may have been generated during specimen preparation.

2.2. Young's modulus measurement as a function of time elapsed after thermal shock

The Young's modulus of the specimens before and after thermal shock was measured via the sonic resonance method [41, 42], in which a specimen is suspended by cotton threads (Fig. 1). One of the threads is attached to a "driver" piezoelectric transducer, while the other thread is attached to a "pick-up" transducer. The driver transducer converts electronic signals from the frequency synthesizer into mechanical vibrations (Fig. 2). Tuning the frequency synthesizer allows one to find a resonant condition of the specimen, which is then sensed by the pick-up transducer. The Young's modulus of the prismatic bar-shaped specimens was calculated from the measured resonant frequencies [41, 43].

An unshocked Macor glass–ceramic specimen was used as a control specimen to guard against a possible systematic "drift" in the transducer response. The

0022–2461

TABLE I Dimensions and densities of materials used in this study

Material	Code	Thickness (cm)	Width (cm)	Length (cm)	Density ($g\,cm^{-3}$)
SiC–AS	RLA 5.22	0.152	1.137	4.92	2.39
	RLA 5.14	0.142	1.510	4.71	2.47
Macor	MA-2	0.179	1.290	7.79	2.52
	MA-3	0.179	1.325	7.79	2.52
	MA-4	0.179	1.337	7.79	2.52
	MA-5	0.179	1.359	7.79	2.51
	MA-6	0.177	1.169	7.83	2.49
Alumina	–	0.105	1.20	7.01	3.49

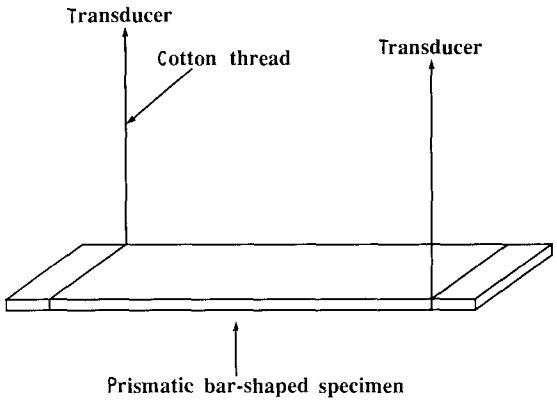

Figure 1 Method of specimen suspension for sonic resonance technique.

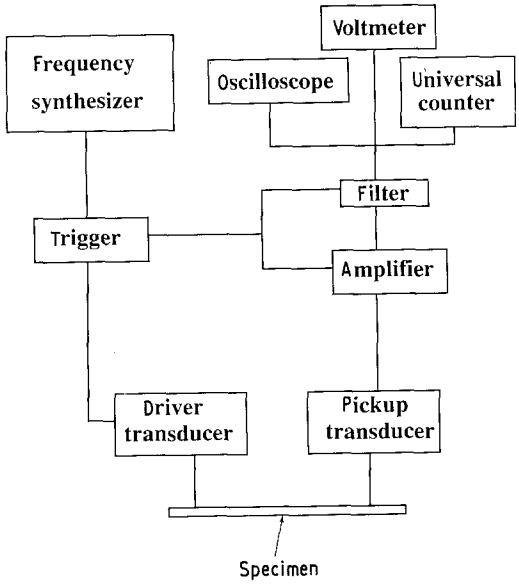

Figure 2 Schematic diagram of sonic resonance system.

modulus of the Macor control specimen was remeasured after every five to six modulus recovery runs. During the entire study, the measured modulus of the control specimen varied by less than $\pm$ 0.0075 GPa (the average modulus of the control specimen was 62.70 GPa), which indicated negligible change in the transducer response over the course of the study.

To induce thermal shock damage, specimens were first held at a preselected temperature for at least 30 min in a vertical-muffle tube electric furnace. The specimens were then quenched into a room-temperature deionized water bath. After drying the quenched specimens with a paper towel, the elastic modulus of the specimens was measured (in air at room temperature) as a function of time for times up to 600 min following the quench. Modulus readings were taken at time intervals of about 15 to 20 min during the first 150 min after the quench and then at intervals of 60 to 90 min during the remainder of the modulus recovery measurement. During the time intervals between the actual modulus measurements, the specimen and suspension threads were supported on a block, so that the transducer would not be subjected to a dead-weight load during the extended period over which the modulus measurements were conducted.

Since the calculation of Young's modulus requires that the specimen mass be known, specimen mass was determined by an electronic analytical balance (Sartorius Analytic A 210P). In order to assess errors in the mass measurements, a working standard was used whenever the mass of the specimen was measured. During the mass determinations and the modulus measurements, the specimens were handled using tweezers in order to minimize mass change by contamination.

3. Results and discussion

3.1. Young's modulus recovery

The Young's modulus versus time data for the SiC fibre–AS composites (Fig. 3), Macor glass–ceramics (Fig. 4) and polycrystalline alumina (Fig. 5) were each fitted to the following empirical equation using non-linear regression analysis [40]:

$$E(t) = E_{t=0} + \Delta E[1 - \exp(-\delta t)] \quad (1)$$

where E is the Young's modulus at time t, $E_{t=0}$ is the Young's modulus at time $t = 0$ (immediately following the thermal quench), $\Delta E = E_{sat} - E_{t=0}$ where $E_{sat} = E(t)$ for large time t (i.e. the "saturated" value of $E(t)$), δ is the modulus recovery time constant determined by non-linear regression on the modulus recovery data, and t is the time (in minutes) elapsed after the thermal shock.

For each specimen of the three thermally shocked materials included in this study, linear regression on the Young's modulus recovery data showed that the modulus recovery with time was described well by Equation 1 (with correlation coefficient higher than

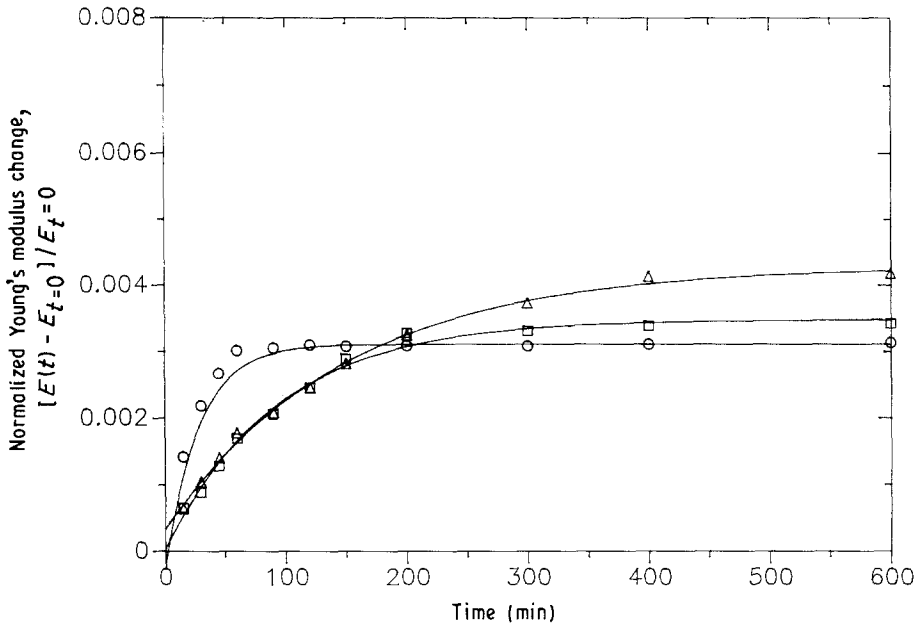

Figure 3 Normalized Young's modulus recoveries as a function of time for SiC fibre–aluminosilicate specimen at $\Delta T = 450\,^{\circ}C$: (○) first shock, (□) fifth shock, (△) tenth shock. Solid curves are least-squares fit to $[E(t) - E_{t=0}]/E_{t=0} = \Delta E[1 - \exp(-\delta t)]/E_{t=0}$.

0.949 for all the modulus versus time data). For each of the three materials, the Young's modulus recovery saturated (levelled off) for times approaching hundreds of minutes, and such saturation behaviour is also in agreement with Equation 1.

For the SiC fibre–AS composites, the modulus recovery time constant δ and modulus $E_{t=0}$ decreased with an increase in the number of thermal shock cycles at a given ΔT (Table II). The observed modulus recovery is very similar to that reported for modulus recovery in thermally shocked polycrystalline yttrium–iron garnet (YIG) [40]. However, for Macor (Table III) and polycrystalline alumina (Table IV), the δ and $E_{t=0}$ values showed no consistent trend as a function of N, the number of thermal shock cycles.

It should be emphasized that for each of the thermal shock cycles for each of the specimens included in this study, the Young's modulus recovery was only partial. Never did the Young's modulus recover entirely to its pre-shocked value (Tables II–IV). In addition, E_{sat}, the value of $E(t)$ for long times t (see Equation 1 and Figs 3–5) decreased (on average) with an increase in the number of thermal shock cycles, N (Tables II–IV). Eventually, E_{sat} tended to a steady-state value as a function of N for each of the three materials included in this study (see Tables II–IV and [13, 14, 16]). The extent of the modulus recovery for a particular thermal shock cycle is shown in Tables II–IV in terms of the ratio $\Delta E/(E_{un} - E_{t=0})$, where E_{un} refers to the unshocked value of Young's modulus. A $\Delta E/(E_{un} - E_{t=0})$ equal to zero would indicate no recovery, while a value of 100% would indicate complete recovery. These ratios ranged from 38.0 to 72.2% for the SiC fibre–AS composites, from 11.4 to 52.0 for the Macor glass ceramics, and from 23.9 to 51.0% for the polycrystalline alumina (Tables II–IV).

3.2. Possible modulus recovery mechanisms

3.2.1. Virtual mass changes due to moisture evaporation

Since the specimens in this study were thermally shocked into a room-temperature water bath, one possible mechanism for the apparent partial modulus recovery might be a time-dependent evaporation of absorbed moisture from the quenched specimen. In order to check for the possibility of a moisture evaporation mechanism, we measured both the mass and the elastic modulus as a function of elapsed time (from the instant of quenching) for a series of thermally shocked Macor specimens. The observed mass of the Macor specimens was then compared with the calculated mass change that would be needed to produce the observed modulus change. Since the existence of

TABLE II Results of non-linear regression analysis of Young's modulus recovery versus time data for SiC fibre–AS composites

Specimen	ΔT (°C)	Unshocked modulus, E_{un} (GPa)	Number of thermal shocks, N	$E_{t=0}$ (GPa)[a]	E_{sat} (GPa)[a]	$\Delta E/(E_{un} - E_{t=0})$ %	δ (min^{-1})[a]
RLA 5.14	450	132.72	1	132.05	132.51	68.7	0.0466
			5	131.70	132.16	45.1	0.0107
			10	131.35	131.87	38.0	0.0066
RLA 5.22	370	125.44	1	125.24	125.36	60.0	0.0061
			3	125.26	125.39	72.2	0.0058

[a] Refer to Equation 1.

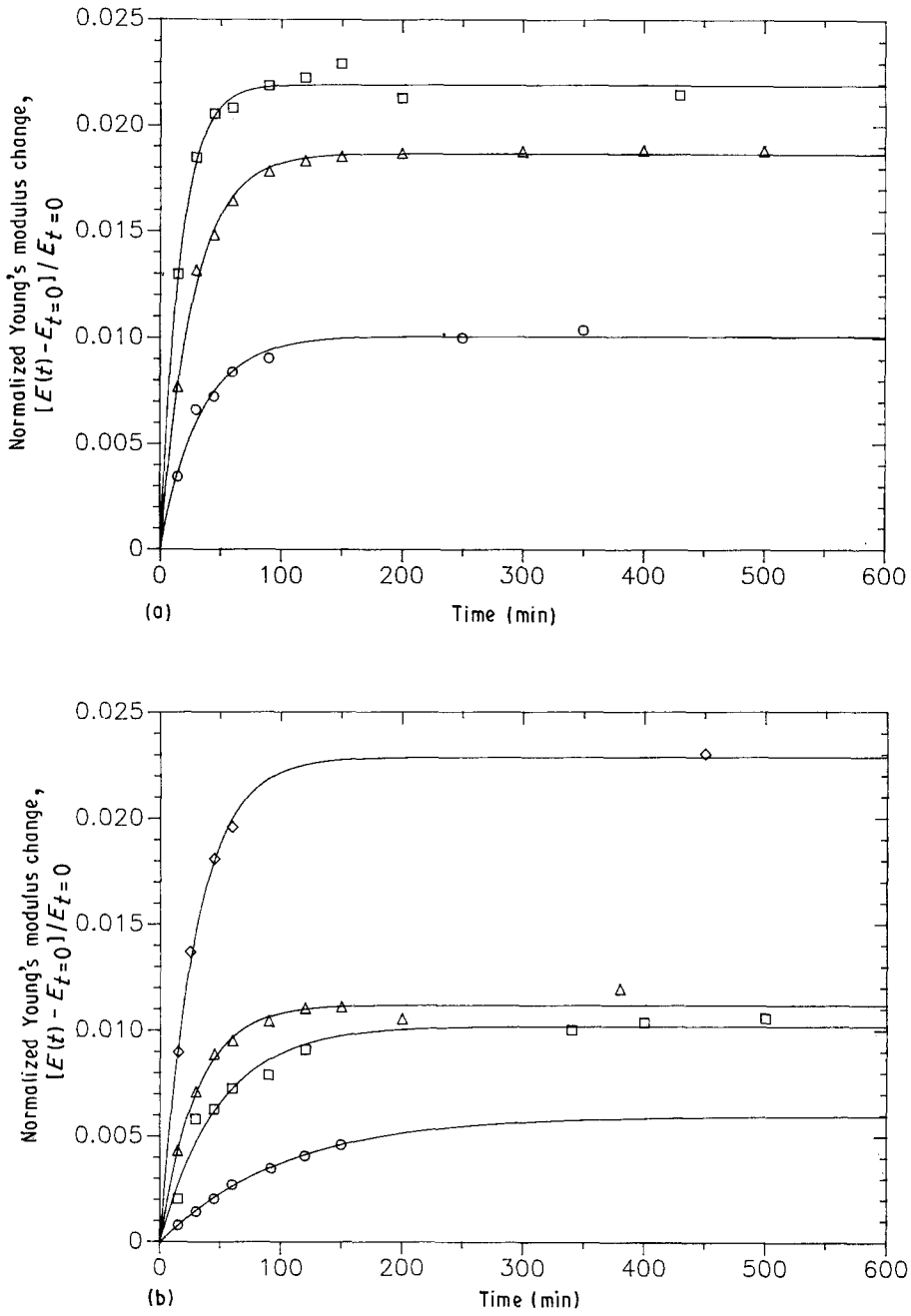

Figure 4 Normalized Young's modulus recoveries as a function of time for Macor glass–ceramic specimen (a) at $\Delta T = 400\,^{\circ}C$, (b) at $\Delta T = 450\,^{\circ}C$: (○) first shock, (□) third shock, (△) fifth shock, (◇) tenth shock. Solid curves are least-squares fit to $[E(t) - E_{t=0}]/E_{t=0} = \Delta E[1 - \exp(-\delta t)]/E_{t=0}$.

such a mass change is in question, we shall refer to the change as a "virtual mass change." In order to calculate the virtual mass change, we began with the expression for the elastic modulus, E, of a prismatic bar-shaped specimen that is appropriate to sonic resonance, our modulus measurement technique [41, 43]:

$$E = \frac{0.946\,42\,L^4 f^2 \rho T}{b^2} \tag{2a}$$

$$= \frac{0.946\,42\,L^3 f^2 m T}{b^3 w} \tag{2b}$$

where L is the specimen length, f is the flexural resonant frequency, ρ is the specimen density, b is the specimen thickness, w is the specimen width, m is the specimen mass and T is the shape factor for the prismatic specimen. The shape factor T is the following function of the specimen dimensions and Poisson's ratio [42]:

$$T = 1 + 6.585(1 + 0.0752\nu + 0.8109\nu^2)(b/L)^2 - 0.868(b/L)^4 - \frac{8.34(1 + 0.2023\nu + 2.173\nu^2)(b/L)^4}{1 + 6.338(1 + 0.14081\nu + 1.536\nu^2)(b/L)^2}$$

where ν is Poisson's ratio.

To determine the virtual mass that could potentially cause the observed modulus recovery, we first solve for the specimen mass, m, in Equation 2b, such that

$$m = \frac{E_{t=0}\, t^3 w}{0.946\,42\,L^3 f^2 T} \tag{3}$$

where $E_{t=0}$ refers to the modulus immediately following the thermal quench.

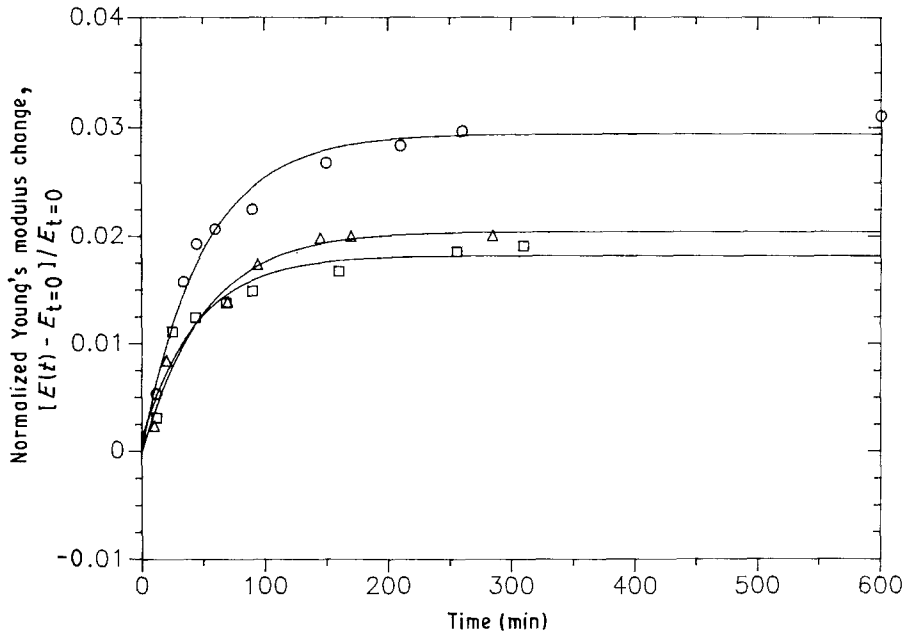

Figure 5 Normalized Young's modulus recoveries as a function of time for polycrystalline alumina specimen at $\Delta T = 250\,^{\circ}C$: (○) third shock, (□) fifth shock, (△) tenth shock. Solid curves are least-squares fit to $[E(t) - E_{t=0}]/E_{t=0} = \Delta E[1 - \exp(-\delta t)]/E_{t=0}$.

TABLE III Results of non-linear regression analysis of Young's modulus recovery versus time data for Macor glass–ceramics

Specimen	ΔT (°C)	Unshocked modulus, E_{un} (GPa)	Number of thermal shocks, N	$E_{t=0}$ (GPa)[a]	E_{sat} (GPa)[a]	$\Delta E/(E_{un} - E_{t=0})$ %	δ (min^{-1})[a]
MA-2	300	63.31	1	61.59	62.42	48.3	0.0413
			3	62.03	62.37	26.6	0.0179
			5	61.96	62.44	35.6	0.0405
			10	62.46	62.81	41.2	0.0199
			20	61.64	62.41	46.1	0.0438
			40	62.06	62.58	41.6	0.0084
			60	61.79	62.58	52.0	0.0445
MA-3	350	63.35	1	61.63	62.14	29.7	0.0129
			3	61.43	62.35	47.9	0.0362
			5	61.77	62.48	44.9	0.0326
			40	61.43	61.98	28.6	0.0204
			60	61.52	62.26	40.4	0.0233
			80	60.92	62.04	46.1	0.0232
MA-4	400	62.43	1	60.65	61.26	34.3	0.0299
			3	59.72	61.03	48.3	0.0598
			5	59.99	61.11	45.9	0.0369
MA-5	450	62.18	1	59.01	59.37	11.4	0.0097
			3	58.11	58.70	14.5	0.0206
			5	58.12	58.77	16.0	0.0332
			10	57.44	58.76	27.8	0.0345
MA-6	500	62.14	1	58.45	59.22	20.9	0.0102
			3	57.45	58.71	26.9	0.0359
			5	57.94	58.67	17.4	0.0268

[a] Refer to Equation 1.

TABLE IV Results of non-linear regression analysis of Young's modulus recovery versus time data for alumina

Specimen	ΔT (°C)	Unshocked modulus, E_{un} (GPa)	Number of thermal shocks, N	$E_{t=0}$ (GPa)[a]	E_{sat} (Gpa)[a]	$\Delta E/(E_{un} - E_{t=0})$ (%)	δ (min^{-1})[a]
Alumina	250	293.95	1	285.0	288.45	41.3	0.0418
			3	278.0	286.14	51.0	0.0202
			5	280.3	285.57	38.6	0.0273
			10	270.6	276.17	23.9	0.0196

[a] Refer to Equation 1.

The virtual masses as a function of time were calculated by inserting the observed resonant frequency data into Equation 3, which thus assumes that the observed resonant frequencies change only as a result of moisture evaporation from the quenched bar. Fig. 6 shows the calculated virtual mass change (due to moisture evaporation) that would be required for the observed modulus changes for Macor specimen quenched at a ΔT of 450 °C. The virtual mass values as a function of time were then fitted to the equation

$$m = m_{t=0} + \Delta m\,[1 - \exp(-\zeta t)] \quad (4)$$

where m is the mass of specimen at time t, $m_{t=0}$ is the mass of specimen at time $t = 0$ (immediately after the thermal quench), Δm = saturated mass $- m_{t=0}$, ζ is a constant determined by non-linear regression, and t is the time (in minutes) elapsed after the thermal shock. The virtual mass changes, Δm, predicted from Equation 4 are two orders of magnitude larger than the measured mass changes for the thermally shocked Macor specimens (Fig. 6).

The mass change of the thermally shocked specimens was thus much too small to account for the observed modulus change, and in fact were smaller than the experimentally determined resolution limits of the electronic mass balance. The coefficient of variation for mass measurements on the control specimen ($= 8.0246 \times 10^{-5}$) was approximately the same as the coefficient of variation for the mass measurements on the thermally shocked specimens. Since the control specimens were not thermally shocked, variations in control specimen masses reflect the experimental scatter in the mass measurements themselves. The thermally shocked specimens' mass change was thus within the experimental scatter of the electronic balance mass measurements.

3.2.2. Microcrack healing

To place our room-temperature crack-healing study in perspective, we shall briefly discuss other crack-healing studies in ceramics. Then we shall compare the crack healing rates found in our study with the rates observed for other ceramic materials.

Mechanisms for microcrack healing can be classified in three different categories [17]: (i) healing by diffusion (thermal annealing) (ii) healing by intermolecular forces (adhesion), and (iii) healing by chemical reaction products. Crack healing by diffusion has been reported for a variety of ceramics, including polycrystalline and single-crystal alumina [18–23], magnesia [20, 24], and urania pellets [25–28]. However, the time-dependent modulus recovery observed in this study occurred at room temperature, so diffusive healing is likely to be insignificant for our specimens.

Crack healing by adhesion can occur at room temperature and has been reported for several materials. In mica, Bailey [31] found that 310 erg cm^{-2} (0.310 J m^{-2}) was required to split mica initially, 190 erg cm^{-2} (0.190 J m^{-2}) was regained on healing, and 250 erg cm^{-2} (0.250 J m^{-2}) was required to resplit the mica. Using double-cleavage drilled compression specimens of soda–lime–silica glass and vitreous silica glasses, Michalske and Fuller [33] measured the strain energy release rate for crack closure and repropagation as a function of ambient relative humidity. Hydrogen-bonded linkage of surface-absorbed water molecules was proposed to account for the experimentally determined strain energy release rate of 0.15 J m^{-2} to reopen healed cracks in humid environments [33]. The relatively high crack repropagation energies (1.7 $\pm$ 0.2 J m^{-2}) under the driest nitrogen atmosphere for soda–lime glass after healing of cracks

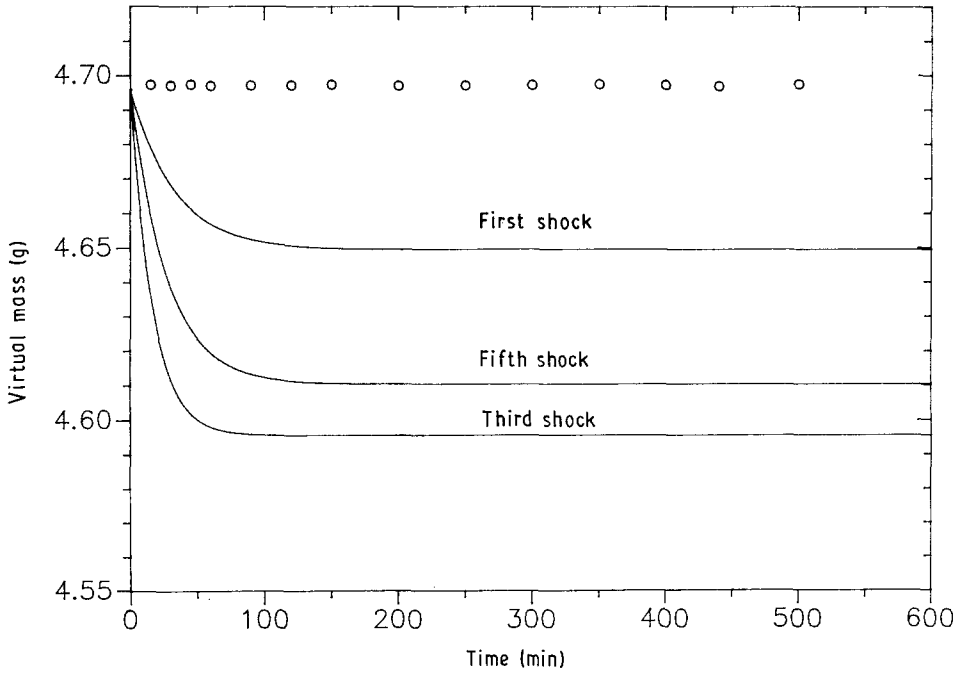

Figure 6 Normalized virtual mass changes equivalent to Young's modulus recoveries for Macor glass–ceramic specimen (ΔT = 400 °C) under the assumption that the observed Young's modulus recoveries are due only to changes in the specimen mass. Solid curves are least-squares fit to $m(t) = m_{t=0} + \Delta m[1 - \exp(-\zeta t)]$. (○) Measured mass; the standard deviation at each point was smaller than the plotting symbol size used in this figure.

was attributed to the formation of either cationic bridges or siloxane bonds between fracture surfaces [33]. Using chevron-notched short-bar specimens, Inagaki *et al.* [35] measured the work of fracture of soda–lime–silica glass as 5.5 $J\,m^{-2}$ in atmospheres of argon and of nitrogen. A work of fracture of 4.4 $J\,m^{-2}$ was found in air. The hysteresis observed in the load versus displacement curve upon loading and unloading the specimen was attributed to crack healing [35]. The crack healing energy, measured from the area inside the load–displacement hysteresis loop, was 0.65 $J\,m^{-2}$ in the inert atmosphere and 0.21 $J\,m^{-2}$ in air [35]. Stavrinidis and Holloway [34] found that no crack closure occurred for soda–lime–silica glass immersed either in dimethylsulphoxide or liquid paraffin, but found that crack closure did occur when specimens were immersed in distilled water. Thus for some ceramics, room-temperature crack healing can occur in humid air as well as in inert atmospheres.

Chemical reaction products can also heal cracks. Pulliam [36] observed crack healing for KCl and NaCl crystals in water and water vapour and attributed the healing to the precipitation of reaction products between crack surfaces. Roach *et al.* [37] found that interfacial layers deposited on crack surfaces in muscovite mica and silicate glass were corrosion products formed by environmental species interacting with the crack surface. For room-temperature testing in air of a heavy-metal fluoride glass, Lehman *et al.* [38] found that Vickers indentation-induced radial cracks decreased in length (apparently healed) as a function of time and relative humidity. The radial cracks from a 0.49 N Vickers indentation impression apparently closed after ageing for 13 days at room temperature in an 85% relative humidity environment (Fig. 2 in [38]). Crack healing in the indented fluoride glass did occur at relative humidities that ranged from 0 to 85%, but as the relative humidity decreased, the observed crack healing rate decreased [38]. Viscous relaxation of the glass around the crack tip, and/or the generation and transport of a fluoride gel phase to the crack aperture, were proposed as possible low-temperature crack closure mechanisms [38]. In a crack healing study of soda–lime–silica float glass in humid environments, Holden and Frechette [39] proposed a crack healing mechanism that proceeded via formation of a moisture-induced gel layer, closure of the crack by stress relief, and gel drying in a controlled atmosphere. Thus, in room-temperature air environments and at a variety of relative humidities, reaction products also can induce crack healing in ceramics.

The time constants, δ, for Young's modulus recovery versus time that were obtained in this study were compared to the crack healing results of other researchers (Table V) [34, 36, 38, 40]. In order to uniformly and systematically compare our data with the data from other researchers, we used a regression equation of the form

$$MPP(t) = MPP_{t=0} + \Delta MPP[1 - \exp(-\Gamma t)] \quad (5a)$$

where $MPP(t)$ is the measured physical property such as crack length, strain energy release rate to repropagate a closed crack, and Young's modulus recovery;

TABLE V Comparison of recovery time constants for elasticity data obtained in this study and calculated time constants for physical properties from other researchers

Material	ΔT (°C)	Time constant (min^{-1})	Method of crack generation	Physical property measured	Reference
SiC–AS	370	0.006[a]	Thermal shock	Young's modulus	This study
	450	0.047[a]	Thermal shock	Young's modulus	This study
Macor	300	0.041[a]	Thermal shock	Young's modulus	This study
	350	0.013[a]	Thermal shock	Young's modulus	This study
	400	0.030[a]	Thermal shock	Young's modulus	This study
	450	0.010[a]	Thermal shock	Young's modulus	This study
	500	0.010[a]	Thermal shock	Young's modulus	This study
Polycrystalline alumina	250	0.042[a]	Thermal shock	Young's modulus	This study
Polycrystalline YIG	165	0.091[b]	Thermal shock	Young's modulus	[40]
KCl[c]		0.028	Cleavage	Length of crack fill-up (crack angle = 2.6×10^{-3} rad)	[36]
NaCl[c]		0.023	Cleavage	Length of crack fill-up (crack angle = 7.5×10^{-4} rad)	[36]
Soda–lime–silica glass		2.333×10^{-4}	Fine scratch and tapping	Strain energy release rate (G)	[34]
Fluoride glass[d]		2.569×10^{-4}	Vickers indentation	Modified radial crack size ($2C - 2a$)	[38]

[a] Recovery data for the first thermal shock cycle at given ΔT.
[b] Specimen edges unbevelled, first thermal shock cycle.
[c] Single crystal, saturated solutions of crystals fed into induced cleavage crack.
[d] ZBLANI (ZrF_4, BaF_2, LaF_3, AlF_3, NaF, InF_3) fluoride glass.

$MPP_{t=0}$ is the measured physical property at $t = 0$; $\Delta MPP = MPP_{sat} - MPP_{t=0}$ where $MPP_{sat} = MPP(t)$ for very large t (i.e. that "saturated" value of $MPP(t)$); Γ is the physical property recovery time constant, as determined by non-linear regression on the physical property recovery data; and t is the time (in minutes) elapsed after the beginning of the recovery measurement.

Note that Equation 5a is identical to our Equation 1 if the physical property measured (MPP) is the Young's modulus, as was the case in our experiment. If we express Equation 5a in terms of a normalized property change, then

$$\frac{MPP_{sat} - MPP(t)}{MPP_{sat} - MPP_{t=0}} = \exp(-\Gamma t) \qquad (5b)$$

Equation 5b emphasizes that the normalized property change is dimensionless and that Γ has units of inverse time. In Table V (as was the case for our modulus recovery analysis), we used min^{-1} as the units for the physical property recovery time constant. In Equation 5a, the term $MPP_{t=0}$ is the initial value ($t = 0$) for measured property MPP in the cracked specimen. $MPP_{t=0}$ is a measure of the extent to which property MPP is affected by the crack(s) in the specimen. Therefore, $MPP_{t=0}$ contains little, if any, information about the crack healing behaviour during recovery. MPP_{sat} measures the "saturated value" of MPP (that is, the limit of $MPP(t)$ for t large). Experimentally, MPP_{sat} can be difficult to determine accurately. For example, it could be difficult to choose an appropriate time cut-off in evaluating MPP_{sat}. However, the recovery time constant, Γ, allows one to quantitatively compare the relative recovery rates of physical properties in terms of a modelled exponential time-dependence of the recovery. Regardless of the physical units of $MPP(t)$, the time-dependence of MPP can be modelled (for Equation 5b) in terms of a single number with reciprocal time units. This, of course, assumes that the property recovery can be described well with Equations 5a or 5b.

The data from other researchers [34, 36, 38, 40] were taken directly from their published plots of property recovery. The recovery time constant Γ was calculated by a non-linear regression fit of Equation 5a to their data. A comparison of the recovery time constants for the elasticity data obtained in this study and the calculated Γ values from other researchers showed that the Γ values are generally in the same range for polycrystalline and single-crystal specimens, while the Γ values for physical property recovery in cracked glass are much lower (Table V).

The physical property recoveries summarized in Table V were determined for a variety of fracture conditions, including cleavage cracks [36], Vickers indentation cracks [38], scribing cracks [34], and cracks induced by thermal shock. However, except for this study and the study of cyclic thermal shock in polycrystalline YIG [40], the fracture conditions involved only a single load cycle (that is, a crack was induced in the specimen, and the crack subsequently healed) without further reloading of the specimen. To express the comparisons in Table V in terms of similar loading histories, the recovery time-constant data from this study (that is, the table entries for SiC–AS, Macor and polycrystalline alumina) represent the modulus recovery rates for the first loading cycle only.

4. Conclusions

Time-dependent partial recoveries in Young's modulus were observed for thermally shocked SiC fibre–AS composites, Macor glass–ceramics and polycrystalline alumina specimens. The observed mass changes for specimens undergoing Young's modulus recovery were found to be two orders of magnitude smaller than the mass changes that would be necessary to account for the observed modulus recovery. Thus mass changes arising from the evaporation of water absorbed during the cyclic thermal quenching of the specimens could not account for the Young's modulus recovery.

The observed Young's modulus recovery in the three ceramic materials is likely to be due to room-temperature microcrack healing. Numerical estimates of property recovery rates were obtained from a regression analysis of available data on room-temperature crack healing in ceramics. The calculated recovery time constants for cleavage cracks in single crystals and for thermal-shock cracks in polycrystalline YIG agreed relatively well with the time constants for modulus recovery determined in the present study (Table V). However, the recovery time-constants for soda–lime–silica and fluoride glasses were approximately a factor of 10^{-2} smaller than single-crystal and polycrystalline time constants.

Although the particular microcrack healing mechanism has not been documented in this study, it is assumed that water or water vapour in the quench medium or in the ambient atmosphere (laboratory air) interacted with the fresh surfaces of cracks induced by cyclic thermal shock. For the materials included in this study, further work is needed to determine whether chemically reactive fresh crack surfaces may promote crack healing via mechanisms such as adhesion or by the build-up of reaction products.

Acknowledgements

The authors acknowledge the financial support of the National Science Foundation under grant No. MSM-8706915 and support by the State of Michigan's Research Excellence Fund. The authors thank Dr Chyung, Corning Glass Works, for the SiC fibre-reinforced aluminosilicate glass–ceramic composites.

References

1. F. DELALE, *Engng Frac. Mech.* **31** (1988) 145.
2. R. W. DAVIDGE and T. J. GREEN, *J. Mater. Sci.* **3** (1968) 629.
3. B. A. BOLEY and J. H. WEINER, "Theory of Thermal Stresses" (Wiley, New York, 1960) Ch. 3.
4. A. H. HEUER, N. CLASSEN, W. M. KRIVEN and M. RUHLE, *J. Amer. Ceram. Soc.* **65** (1982) 642.
5. Y. FU, A. G. EVANS and W. M. KRIVEN, *ibid.* **67** (1984) 626.

6. E. D. CASE, K. M. LOUIE and A. G. EVANS, *J. Mater. Sci. Lett.* **3** (1984) 879.
7. H. P. KIRCHNER and E. D. ISSACSON, *J. Amer. Ceram. Soc.* **65** (1982) 55.
8. H. P. KIRCHNER, *ibid.* **67** (1984) 347.
9. H. OHIRA and R. C. BRADT, *ibid.* **71** (1988) 35.
10. W. P. ROGERS, A. F. EMERY, R. C. BRADT and A. S. KOBAYASHI, *ibid.* **70** (1987) 406.
11. K. MATSUSHIDA, S. KURATANI, T. OKAMOTO and M. SHIMADA, *J. Mater. Sci. Lett.* **3** (1984) 345.
12. S. NISHIJIMA, K. MATSUSHITA, T. OKADA, T. OKAMOTO and T. HAGIHARA, in "Nonmetallic Materials and Composites at Low Temperature 3", edited by G. Hartwig and D. Evans (Plenum, New York, 1986) pp. 143–151.
13. Y. KIM, W. J. LEE and E. D. CASE, in "Metal and Ceramic Matrix Composites: Processing, Modeling and Mechanical Behavior", edited by R. B. Bhagat, A. H. Clauer, P. Kumar and A. M. Ritter (Minerals, Metals and Materials Society, Warrendale, OH, 1990) pp. 479–486.
14. *Idem.*, in Proceedings of the American Society for Composites 5th Technical Conference, June 1990, East Lansing, MI (Tectonic Publishing Co., Lancaster, PA, 1990) pp. 871–81.
15. W. J. LEE and E. D. CASE, *Mater. Sci. Engng* **A119**: (1989) 113.
16. *Idem., J. Mater. Sci.* in press.
17. E. D. CASE, J. R. SMYTH and O. HUNTER Jr, in "Fracture Mechanics of Ceramics", Vol. 5, edited by R. C. Bradt, A. G. Evans, D. P. H. Hasselman and F. F. Lange (Plenum, New York, 1983) pp. 507–530.
18. T. K. GUPTA, *J. Amer. Ceram. Soc.* **59** (1976) 259.
19. *Idem., ibid.* **61** (1978) 191.
20. *Idem., ibid.* **59** (1976) 448.
21. A. G. EVANS and E. A. CHARLES, *Acta Metall.* **25** (1977) 919.
22. C. F. YEN and R. L. COBLE, *J. Amer. Ceram. Soc.* **55** (1972) 507.
23. F. F. LANGE and K. C. RADFORD, *ibid.* **53** (1970) 420.
24. T. K. GUPTA, *ibid.* **58** (1975) 143.
25. J. T. A. ROBERTS and B. J. WRONA, *ibid.* **56** (1973) 297.
26. G. BANDYOPADHYAY and J. T. A. ROBERTS, *ibid.* **59** (1976) 415.
27. G. BANDYOPADHYAY and C. R. KENNEDY, *ibid.* **60** (1977) 48.
28. R. N. SINGH and J. L. ROUTBORT, *ibid.* **62** (1979) 128.
29. Y. OHYA, Z. NAKAGAWA and K. HAMANO, *ibid.* **71** (1988) c-232.
30. M. TOMOZAWA, K. HIRAO and P. E. BEAN, *ibid.* **69** (1986) c-186.
31. A. I. BAILEY, *J. Appl. Phys.* **32** (1961) 1407.
32. R. B. LEONESIO, *J. Amer. Ceram. Soc.* **55** (1972) 437.
33. T. A. MICHALSKE and E. R. FULLER, *ibid.* **68** (1985) 586.
34. B. STAVRINIDIS and D. G. HOLLOWAY, *Phys. Chem. Glasses* **24** (1) (1983) 19.
35. M. INAGAKI, K. URASHIMA, S. TOYOMASU, Y. GOTO and M. SAKAI, *J. Amer. Ceram. Soc.* **68** (1985) 704.
36. G. R. PULLIAM, *ibid.* **42** (1959) 477.
37. D. H. ROACH, S. LATHABAI and B. R. LAWN, *ibid.* **71** (1988) 97.
38. R. L. LEHMAN, R. E. HILL Jr and G. E. SIGEL Jr, *ibid.* **72** (1989) 474.
39. M. K. C. HOLDEN and V. D. FRECHETTE, *ibid.* **72** (1989) 2189.
40. H. M. CHOU and E: D. CASE, *Mater. Sci. Engng* **100** (1988) 7.
41. G. PICKETT, *ASTM Proc.* **45** (1945) 846.
42. E. SCHREIBER, O. L. ANDERSON and N. SOGA, "Elastic Constants and Their Measurement" (McGraw-Hill, New York, 1974) Ch. 4.
43. D. P. H. HASSELMAN, "Tables for the Computation of Shear Modulus and Young's Modulus of Rectangular Prisms" (Carborundum Co., Niagara Falls, New York, 1961).

Received 14 November 1990
and accepted 10 April 1991